Springer

Journal of
Mechanical
Science and
Technology

Journal of Mechanical Science and Technology 22 (2008) 171~179

www.springerlink.com/content/1738-494x

Propulsive characteristics of dual fish-like foils

Cheolheui Han[1], Hakjin Lee[2] and Jinsoo Cho[3,*]

[1]*Chungju University, Chungju, 143-701, Korea*
[2]*Sindoricoh Corporation, Seoul, 133-120, Korea*
[3]*Hanyang University, Seoul, 133-791, Korea*

(Manuscript Received October 23, 2006; Revised August 12, 2007; Accepted August 20, 2007)

Abstract

The effect of the vertical and horizontal distances between dual fish-like foils on the propulsive characteristics of the biomimetic propulsor system is investigated by using an unsteady panel method. The present method is validated by comparing computed results with other numerical and experimental data. The mutual vortex-vortex interaction between the shed vortices from both foils has the effect of changing the pointing direction of mushroom heads. The leading foil's propulsive characteristics do not change much with the vertical distance between the foils, whereas the following foil's propulsive characteristics are changed significantly depending on the vertical and horizontal distances between the foils. The overall wake patterns depend mainly on the horizontal distance. The intensity of the mutual interaction between the wake vortices depends on the vertical distance. Thus, the propulsive characteristics of the dual fish-like foils are complicated functions of the vertical and horizontal distances between the foils. The present method has the limitation of potential-low assumption. If the flow separation near the leading edge of the foils is not significant, the present method can be applied to the design of biomimetic propulsors.

Keywords: Unsteady panel method; Biomimetics; Fish-like foils; Fish swimming

1. Introduction

Aerial and marine creatures in nature flap or undulate their foils in order to obtain the necessary fluid-dynamic forces for locomotion. Recent progress in material science and technology has led to the possible development of aerial or marine vehicles using biomimetic foils. Extensive reviews on flapping foils and their applications to the development of aerial or marine vehicles were given by Rozhdestvensky and Ryzhov [1] and Ho et al. [2], respectively. Among the biomimetic foils, the foils of live fish have obtained considerable attention from many investigators because of marine creatures' outstanding swimming performances. Sfakiotakis et al. [3] reviewed the fish swimming modes following the Breder's classification scheme: 1) Body and/or Caudal Fin movement (BCF), 2) Median and/or Paired Fin propulsion. Bandyopadhyay [4] described the progress in biorobotic autonomous undersea vehicles and reviewed the trends in the fish locomotion research. The basic understanding of fish propulsion was also applied to the development of a robotic fish [5].

To develop aerial or marine vehicles or robots with good performance and maneuverability, it is necessary to understand the flow physics about the biomimetic foils in nature. The basic propulsion mechanism of heaving and/or pitching foils has been known as follows: the shed wake from the foil's trailing edge is developed as the staggered array of vortices with reverse direction of rotation to a von Karman vortex street, and these vortices induce jet-like flows (known as the Knoller-Betz effect) [6-9]. According to the experimental study of Lai and Platzer [10], mushroomlike vortices pointing upstream indicate a drag-

*Corresponding author. Tel.: +82 2 2220 0429, Fax.: +82 2 2281 4016
E-mail address: chhan@cjnu.ac.kr
DOI 10.1007/s12206-007-1021-x

producing wake, whereas mushroom-like vortices pointing downstream indicate thrust-producing wake. Jones et al. [11] showed that the formation and evolution of unsteady reverse von Karman vortex streets is fundamentally an inviscid phenomenon over a broad range of Strouhal numbers. Unlike the foils of birds or insects, the body and caudal fin of fish undulates as a traveling wave. The tail of some of the fastest swimming animals resembles a high aspect ratio foil, which has led to theoretical and numerical studies [5]. The tip of the tail fin produces the reverse von Karman vortex streets, which results in the thrust generation. Han et al. [12] investigated the propulsive characteristics of a single fish-like foil in undulation motion.

Most of the previous works have focused on the hydrodynamic analysis of a single foil of various kinds. The study on the hydrodynamic characteristics of multiple foils is important in the energy-harvesting aspect of schooling fish and the design of biomimetic propulsors. The complicated vortex-vortex interaction behind schooling fish has not been investigated much. When two foils operate side by side, the vortex-vortex interaction behind the foils can be beneficial to the performance of two-foil systems. Sfakiotakis *et al*. [3] mentioned that "vorticity control mechanisms were originally proposed in the early 1970's in the context of fish schooling behavior often observed in scombrids." If the fish stay close together, a "channeling effect" causes a favorable flow at the sides of the vortex-street. It was also mentioned that "the advantage of fish schooling is greater when the fish in the same column swim in anti-phase with the neighbors. These requirements point to an elongated diamond-shape pattern as the basic optimum structures in fish schools." Several investigators calculated the hydrodynamic characteristics of fish schooling by simply modeling the wake vortices as a staggered array of vortices [13, 14].

Regarding the development of biomimetic multiple propulsors system, Bandyopadhyay et al. [15] investigated the swimming hydrodynamics of a pair of flapping foils to the tail of a rigid body. Akiyama *et al*. [16] observed that flow fields around vibrating plates created counter rotating vortices. Researchers at MIT showed that two flapping airfoils produce larger thrust than a propeller. According to Jones et al. [11], when the foils are placed in a biplane configuration, this configuration is similar to a single foil in ground effect and is more efficient and thrust-producing than a single foil. Han et al. [17] investigated the thrust characteristics of two flat plates in pitch oscillation. They found that two plates in the opposite phase produced larger thrust than two plates in the same phase.

The main purpose of present paper is to understand the propulsive characteristics of dual fish-like foils in undulation motion and to reveal the relation between the wake vortices and the propulsion forces. An unsteady panel method developed for a single fish-like biomimetic foil [12] is extended to the case of dual fish-like foils. The propulsive characteristics of the dual fish-like foils are investigated by changing the horizontal and vertical distances between the foils.

2. Unsteady panel method

Two coordinate systems are used in order to describe the unsteady motions of biomimetic foils moving through a stationary fluid medium (See Fig. 1). One is a body-fixed coordinate system (x, y). The other is the inertial frame of reference (X, Y). It is assumed that the viscous effect is confined within a thin boundary layer. Thus, the flow is assumed to be inviscid, incompressible and irrotational over the entire flow field, excluding the foils' boundaries and their wakes [18].

The isentropic flow around the deforming foils can be solved by using the continuity equation coupled with energy equation. For an irrotational flow, a velocity potential can be defined in the inertial frame. Then, the continuity equation becomes the Laplace equation of the velocity potential. Mass should be conserved regardless of the coordinate systems. Therefore,

$$\nabla^2\Phi = 0 \quad \text{(in a body-fixed coordinate system)} \qquad (1)$$

Each foil's surface is discretized into N equal length panel elements. The vorticity on each element is considered to be linear. The vorticity of linear

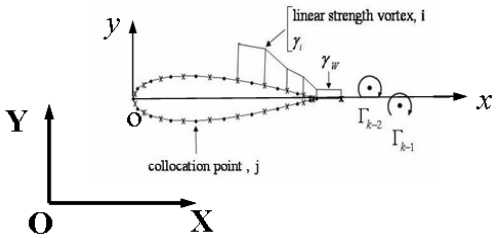

Fig. 1. Nomenclature of the present method.

strength on each element is represented as

$$\gamma(x) = \gamma_j + \gamma_{j+1}(x - x_{j+1}) \tag{2}$$

The wake is represented by free vortices which deform freely by the assumption of a force-free position during the simulation. The free vortices are connected to the bound vortices at the trailing edge of each foil through the Kutta condition. The Kutta condition is valid as long as the foil's trailing edge moves with small or moderate amplitude and frequency. The strengths of the elementary solutions are obtained by enforcing boundary conditions as follows.

A. The flow disturbance, due to the foil's motion through the fluid, should vanish far from the plates. This boundary condition can be satisfied automatically by using the vortices as the singularity distributions.

B. Zero normal flow across the foils' solid boundaries. The continuity Eq. (1) does not directly include time-dependent terms. Time dependency is introduced through the modification of "zero normal flow on a solid surface" and the use of the unsteady Bernoulli equation. The kinematic velocity ($\vec{v}$) is given as follows,

$$\vec{v} = -[\vec{V}_0 + \vec{v}_{rel} + \vec{\Omega} \times \vec{r}] \tag{3}$$

where $\vec{V}_0$ is the velocity of the body-fixed system's origin, $\vec{r}$ = (x, y, z) is the position vector, $\vec{\Omega}$ is the rate of rotation of the body's frame of reference. The additional relative motion within the body-fixed coordinate system is represented as $\vec{v}_{rel}$. The zero-velocity normal to a solid surface boundary in the body-fixed frame becomes

$$(\nabla\Phi - \vec{V}_0 - \vec{v}_{rel} - \vec{\Omega} \times \vec{r}) \cdot \vec{n} = 0$$

(in a body-fixed coordinate system) (4)

where $\vec{n}$ is the normal to the body's surface, in terms of the body-fixed coordinates (x, y). Fulfilling the boundary condition on the surface requires that, at each collocation point, the normal velocity component will vanish and we can write Eq. (4) as

$$\left(\sum_{j=1}^{N+1} A_{ij}\gamma_i + A_{iN+2}\gamma_w \right) \cdot \mathbf{n}_i = -\left(\mathbf{V}(t) + \mathbf{V}_{iw} \right) \cdot \mathbf{n}_i$$

on the foil for i=1, 2, ..., N (5)

where the influence matrix element A_{ij} represents the normal velocity component at a control point i by the vortex (having a unit circulation) at the panel element j . The elements a_{ij} are functions of geometry. Γ_j is the unknown circulation of the point vortex representing the vorticity of the panel element j . q_i represents the normal velocity component induced at control point i by the starting vortex and its image. $\vec{V}_{wi}$ is the velocity induced by the wake vortices and their images whose positions and circulations are known. At the beginning, $\vec{V}_{wi}$ is zero. The calculation begins at t = Δt and the wake at this moment consists of a single vortex Γ_c . Following Mook et al. [19], we simulate the starting vortex by placing it at a point l/4 l behind an airfoil trailing edge (Fig. 2).

C. Kelvin condition. The use of the Kelvin condition that the circulation around a fluid curve enclosing the plates and their wakes is conserved, will supply an additional equation.

$$\frac{(\Delta l_1)}{2}(\gamma_1)_k + \sum_{i=1}^{N}\left[\frac{(\Delta l_{i-1}) + (\Delta l_i)}{2}(\gamma_i)_k\right] + \frac{(\Delta l_N) + (\Delta l_w)}{2}(\gamma_{N+1})_k + \frac{(\Delta l_w)}{2}(\gamma_w)_k = \sum_{k=1}^{NT-1}\Gamma_{k-1} \tag{6}$$

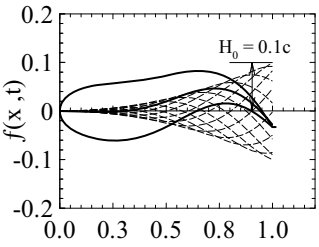

(a) Geometrical representation of a fish-like foil

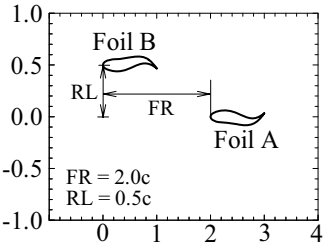

(b) Nomenclature of dual fish-like foils

Fig. 2. Geometrical representation and nomenclature of dual fish-like foils.

where Δl and Δl_w represent panel element length of the body and its wake. NT is the number of total time steps and Γ_{wake} is the circulation of a wake core at node k, which is zero at the start of motion. The wake is created as a result of shedding and convecting the starting vortex at each time step.

D. The unsteady Kutta condition. This condition at the trailing edge of a plate is satisfied by shedding the vorticity generated at the trailing of a plate at the local fluid particle velocity.

E. Continuous pressure across the wake. This condition is fulfilled with convecting wakes downstream at the local fluid particle velocity.

To find the solutions of Eq. (5), an initial condition describing the position of the wake and its vorticity must be prescribed. At each time step, a newly shed starting vortex is fixed at a point l/4 l behind a plate's trailing edge as required by the unsteady Kutta condition. All the circulation strengths are determined including the effects of their images by Gauss elimination. At the end of each time step, the shed vortex is convected downstream to its new position at the local fluid particle velocity. The procedure is repeated for any desired number of time steps.

2.1 Wake rollup

Since the wake is force-free, each vortex representing the wake must move with the local flow velocity. The local flow velocity is the result of the velocity components induced by the wake and the plate. It is measured in the inertial frame of reference (X, Y). To achieve the vortex wake rollup at each time, the induced velocity $(u,v)_i$ at each vortex wake point i is calculated, and then the vortex elements are moved by a 4th-order Runge-Kutta convection scheme. In the regions where vortex cores are separating, leaving big gaps and beginning to reassemble, the unequal spacing between the cores can lead to numerical instabilities [19]. The core addition scheme imitates the elongated region of the vorticity in the actual flow. If the distance between two successively shedding cores is separated by more than a prescribed "critical length", a new core is located at the midpoint of the line segment connecting them. This new core has one-third the sum of circulations around the two original cores. The circulations around the two original cores are reduced by a factor of two-thirds. The velocity within the core (v_j) with a core radius r_c at time t is

$$v_j = \frac{\Gamma_j}{2\pi r}\left\{1-\exp\left[-1.25643\left(\frac{r}{r_{cj}}\right)^2\right]\right\} \tag{7}$$

where Γ_j is a strength of a vortex and r is the distance between the origin of the vortex core and the point in space. Outside the core region, the induced velocity can be taken as that of a free vortex of strength Γ_j.

The 4th-order Runge-Kutta convection scheme is as follows:

$$\begin{aligned}
&\mathbf{r}_{k+1} = \mathbf{r}_k + \frac{1}{6}\left[a_1 + 2(a_2 + a_3) + a_4\right]\Delta t \\
&a_1 = f(t,r) = \left(\frac{\partial r}{\partial t}\right)_k,\ a_2 = f\left(t+\frac{\Delta t}{2}, r + a_1\frac{\Delta t}{2}\right) \\
&a_3 = f\left(t+\frac{\Delta t}{2}, r + a_2\frac{\Delta t}{2}a_2\right),\ a_4 = f\left(t+\Delta t, r + a_3\Delta t\right)
\end{aligned} \tag{8}$$

2.2 Computation of aerodynamic loads

In the body fixed frame, thrust (or drag) is calculated by using the momentum conservation theorem.

$$T(or\ D) = \rho\int_{-\infty}^{\infty} V(y)\left[V(y) - U_\infty\right]dy \tag{9}$$

where $V(y)$ is the velocity profile at the cross section behind a chord length from the plate's trailing edge, and U_∞ is the freestream velocity. Time-averaged thrust coefficient can be defined as follows.

$$\overline{C_T} = \frac{1}{T}\int_0^T C_T dt \tag{10}$$

where T is the period of the undulation.

3. Results and discussion

Han et al. [12] investigated the propulsive characteristics of a single fish-like foil by changing swimming modes that are represented by the undulation frequency. Thus, the undulating frequency of $\omega c/U_\infty$ =5 and maximum thickness of 0.12C is set by following the results by Han et al. [12]. As shown in Fig. 2, the geometrical representation of dual fish-like foils at each time can be expressed by using the geometrical definition of conventional airfoils. The mean camber line of each foil is represented as

$$f(x,t) = H_0 x^2 \cos\omega(x/U_\infty - t) \tag{11}$$

where H_0x^2 is the undulation amplitude envelope of the wave, c is the chord length and ω is the undulation angular frequency. H_0 represents the maximum amplitude of the tail fin. In this paper, the chord length is assumed to be 1.0 m. After the mean camber line is determined, the thickness distribution of the foil is added to the mean camber line. In the present study, it is assumed that the foils have the thickness distribution of a NACA 0012 airfoil.

As shown in Fig. 3, the present method is validated by comparing simulated wake shapes behind plunging airfoils with particle tracing by using the finite element method [20]. The reduced frequency ($k=\omega c/U_\infty$) is set to 2.0. The plunging amplitude of both foils ($h_{0)}$ is set to 0.4C. The vertical distance between the foils (y_0) is 1.4C. Fig. 3 shows that overall wake patterns by the present method agree with those by CFD. In Fig. 3(a), it is also shown that the flow is separated from the leading edges of both foils. The separated leading edge vortices (LEV) are interacting with trailing edge vortices (TEV), which results in the complicated wake patterns. Thus, it can be deduced that the effect of vortex-vortex interaction should be considered in order to accurately predict the aerodynamic characteristics of plunging foils. However, it is not included in the present method.

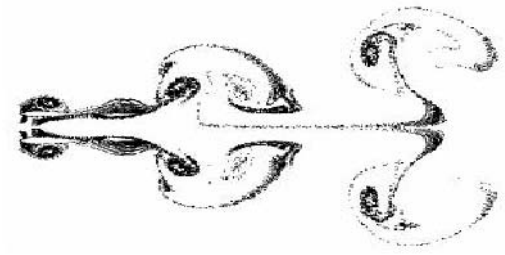

(a) Particle traces of CFD

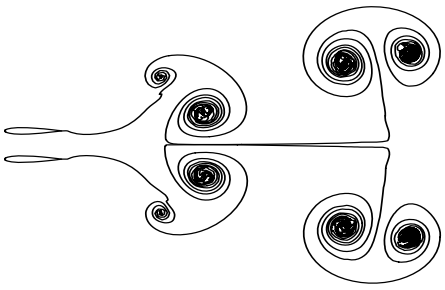

(b) Present result

Fig. 3. Comparison of a wake pattern behind plunging airfoils for k=2, h0=0.4, and y0=1.4.

As shown in Fig. 4, the present method is also validated by comparing the computed thrust coefficients with those by CFD [20]. Fig. 4(a) shows the time history of thrust coefficient of a rigid foil in heave oscillation. The thrust coefficient is plotted as a function of the nondimensional time. The peak value in the thrust coefficients is obtained when the foil is at the end of up or down strokes or in the middle of both strokes. At the end of each stroke, the flow is separated from the leading edge of the foils and then the separated leading edge vortices interact with the trailing edge vortices. The vortex-vortex interaction between the LEV and TEV significantly affects the resulting fluid dynamic characteristics. Fig. 4(b) shows the time averaged thrust coefficients of dual rigid foils oscillating with the reduced frequency range of 0<k<2. It can be deduced from the figures that the present results are qualitatively in good agreement with CFD results at low frequency [20]. However, there are discrepancies between the present results and those by CFD at higher frequency (k>1.0). This is due to the shortcoming of the present method which does not include a numerical scheme for the leading edge separation.

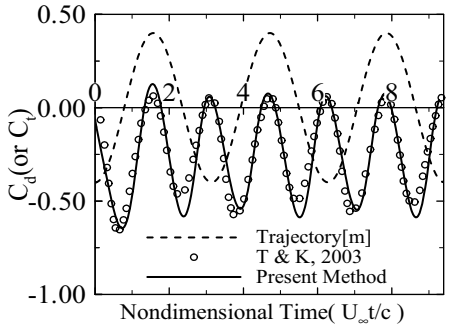

(a) Time histroy of Cd(or Ct)(k=2)

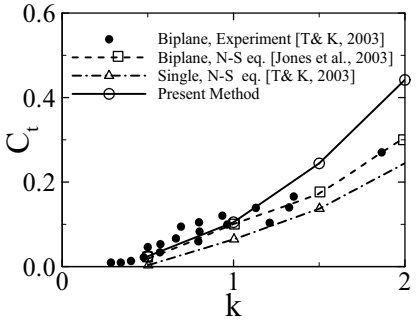

(b) Time averaged thrust coefficient

Fig. 4. Propulsive characteristics of rigid plunging airfoils($\Delta t=\pi/100$, $L_{cr}=3.0\Delta tU_\infty$, $r_c=0.07$, $h_0=h/c=0.4$).

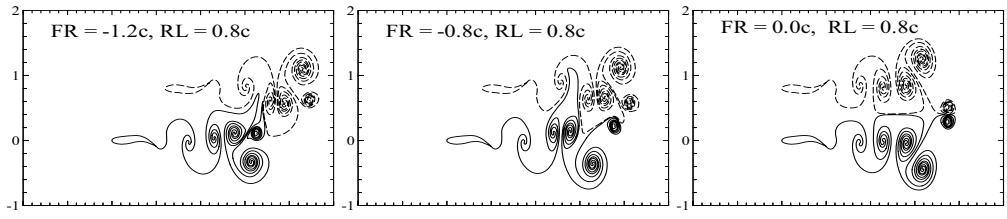

(a) Wake shapes

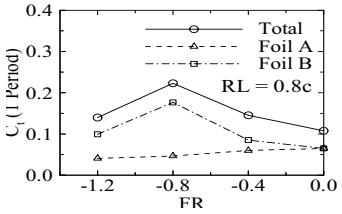

(b) Time-averaged thrust coefficient

Fig. 5. Effect of the horizontal distance between the fouls (RL=0.8e)

As shown in Fig. 3 and Fig. 4, the present method is validated for a rigid foil or foils in heave oscillation. The shortcoming of the present method that does not include the leading edge vortex separation in the current numerical scheme results in the discrepancy with CFD results [20]. However, in the present study of dual fish-like foils, the leading edge part of the foil will not oscillate but retain its shape unlike the plunging rigid foils. Only rear body and tail fin will change their shapes as a progressive wave form. Thus, it is assumed that the shortcoming of the present method does not cause the accuracy problem except when the wake vortices from the leading foil induce flow separation in the following foil. The investigation of the vortex-induced effect will require a complicated computation using Navier-Stokes equations.

Fig. 5 shows the wake patterns and time-averaged thrust coefficients of dual fish-like foils which are moving with uniform velocity (U_∞=1.0 m/s). Both foils wiggle their rear body parts and tail fins with anti-phase while head parts maintain their shape. The vertical distance between the foils is fixed as RL=0.8C. In Fig. 5(a), the wake shapes behind the foils are plotted for several horizontal distances between the foils (FR=-1.2C, -0.8C, and 0.0C). According to the experimental study of Lai and Platzer [10], the pointing direction of mushroom heads indicates the propulsive characteristics of a plunging foil (thrust-producing with mushroom head pointing downstream and drag-producing with mushroom head pointing upstream). If both foils are moving in parallel (FR=0.0), the wake shapes behind the foils show a symmetric pattern with respect to the central line between the foils. Thus, it can be deduced that one of dual foils moving parallel to each other with close vertical distance between them behaves like a single foil in ground effect. When the foil A is leading the foil B (FR=-1.2C and -0.8C), the wake vortices behind the leading foil are pulled into the space in-between core vortices from the trailing foil. Then, the pulled-up vortices change the pointing direction of mushroom heads into the downstream direction. The mutual interaction of the vortices (which is a function of horizontal distance between the foils) has the effect of changing the pointing direction of mushroom heads from thrust-producing toward drag-producing. In Fig. 5(b), the time-averaged thrust coefficients of the foils are plotted as a function of horizontal distance (FR) between the foils. Within the investigated range of FR from -1.2C to 0.0C, the time averaged thrust coefficient of the following foil is larger than that of the leading foil except FR=0.0C. The following foil harvests energy contained in the wake vortices generated by the leading foil. The mutual interaction between the vortices is also a function of the Strouhal number that characterizes the vortex-shedding frequency and the distance between the vortices. The maximum thrust of the results in Fig. 5 is obtained when FR=±0.8C at RL=0.8C.

Fig. 6 shows the effect of vertical distance between the foils on the propulsive characteristics of the dual fish-like foils that are moving forward in parallel (FR=0.0) (See Fig. 6(a) for wake patterns and Fig. 6(b) for propulsive characteristics). In Fig. 6(a), the

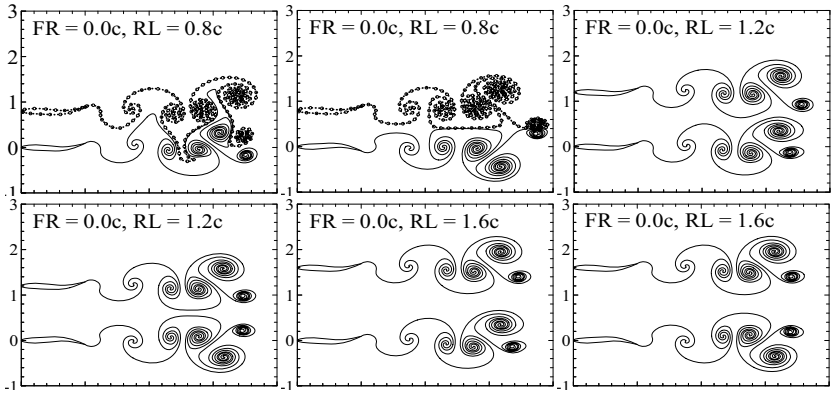

(a) Wake shpes(left-hand side column: in-phase, right-hand side column: anti-phase)

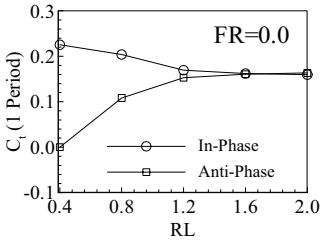

(b) Total thrust coefficient

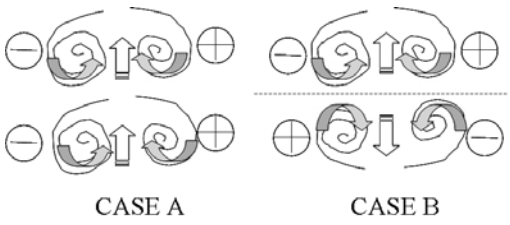

(c) Vortex systems

Fig. 6. Effect of the vertical distance between the foils at FR=0.0C.

left-hand side figures represent the wake patterns behind the foils undulating with in-phase (CASE A), whereas the right-hand side figures show the wake patterns behind the foils undulating with anti-phase (CASE B). When the foils are vertically separated far enough (RL=2.0C), the wake vortices behind the foils do not interact with each other. The mutual interaction of wake vortices is a function of the distance between the vortices because the induced velocity from the other vortices is proportional to 1/r [18]. The wake patterns in CASE A show the mushroom heads of both upper and lower rows pointing in the same direction, whereas the wake patterns in CASE B show the mushroom heads of the upper and lower rows pointing in the opposite direction with respect to each other. With the vertical distance between the foils is less than RL=1.6C, the mushroom heads of CASE A and CASE B are moving toward downstream and upstream, respectively. The total thrust of the propulsor system increases in CASE A and decreases in CASE B with the vertical distance stepping down. Note that each foil in CASE B corresponds to a single foil in ground effect. When a single fish-like foil is moving near the ground, the single foil cannot obtain the beneficial effect of undulation on the thrust generation (which is the similar result as shown Fig. 5 for FR=0.0C). As shown in Fig. 6(c), the rotation of alternately shed vortices (which represent the mushroom head) is opposite to each other. The rotation of two counter-rotating vortices in the upper row is the same as that of the vortices in the lower row in CASE A. The rotation of the vortices in the upper row is opposite to that in the lower row in CASE B. Thus, the two counter-rotating vortices in the upper row of CASE A pull up the vortices in the lower row into the space between the vortices, which results in the rotation of the mushroom heads toward downstream with the vertical distance stepping down. The induced velocities by the vortices in the upper row of CASE B are limited by the imaginary ground that are made by the four vortex systems. Thus, the mushroom heads rotate toward upstream with the vertical distance stepping down, which results in the decrease in the total thrust of the propulsor system.

In Fig. 7, the dual fish-like foils are moving forward with the foil A leading the foil B. Both Fig. 7(a) and Fig. 7(b) show the wake patterns behind the foils and the time-averaged thrust coefficients of the foils, respectively. The left-hand side figures in Fig. 7(a) show the wake patterns behind the foils undulating

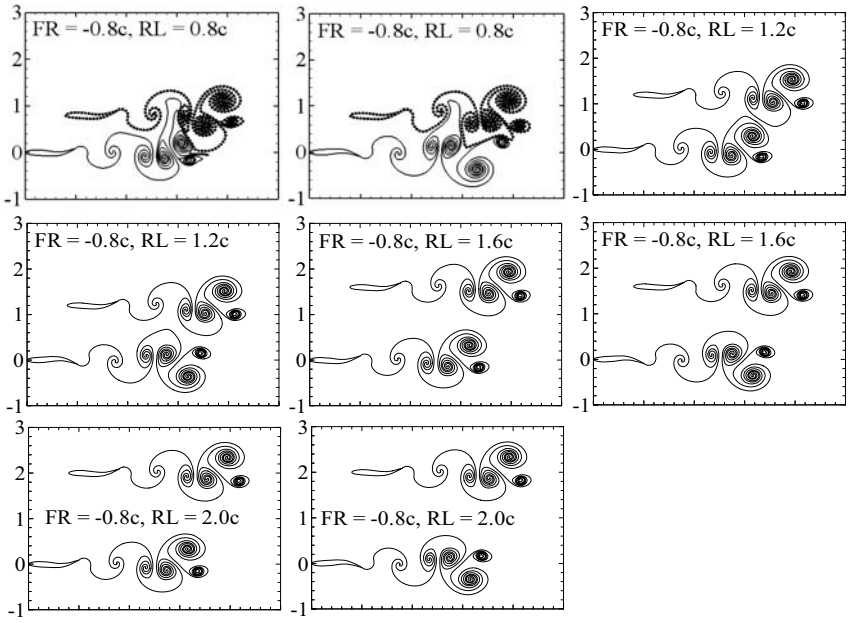

(a) Wake shapes(left-hand side column: in-phase, right-hand side column: anti-phase)

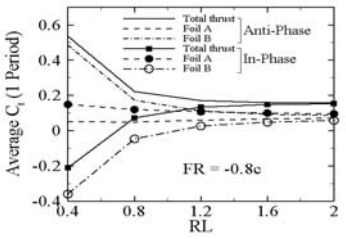

(b) Thrust coefficient

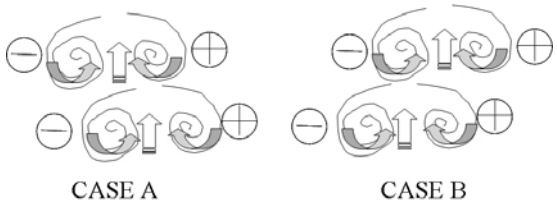

(c) Vortex systems

Fig. 7. Effect of the vertical distance between the foils at FR=-0.8C.

with the in-phase (CASE A), and the right-hand side figures in Fig. 7(a) represent the wake patterns behind the foils undulating with anti-phase (CASE B). Fig. 7(c) shows the vortex systems of both cases (CASE A and CASE B). Like the mushroom heads aligned together in Fig. 6, the mushroom heads in Fig. 7 are arranged staggered due to the horizontal distance between the foils (FR=0.0 in Fig. 6). It can be said that the overall wake patterns depend on the horizontal distance between the foils regardless of undulating phases between the foils. It is also noticeable that the wake vortices in the lower row of CASE B in Fig. 7 are pulled up into the space between the vortices in the upper row. As shown in Fig. 7(b), the total thrust of the propulsor system in CASE B increases, whereas the total thrust in CASE A decreases with the vertical distance stepping down. It can be said that the intensity of the mutual interaction between the wake vortices depends mainly on the vertical distance between the foils. Thus, the overall wake patterns and the mutual interaction between the wake vortices are a complicated function of horizontal and vertical distances, which are critical parameters together with other parameters such as undulation phase and Strouhal number.

4. Conclusions

An unsteady panel method is developed and validated by comparing the computed wake patterns and thrust characteristics of plunging foils with those by finite element method. The wake patterns and thrust characteristics of dual fish-like foils are investigated by changing the vertical and horizontal distances between the foils undulating with in-phase and anti-phase.

It is shown that both vertical and horizontal distances between the dual fish-like foils affect significantly the propulsive characteristics of the dual fish-like foils. The overall wake patterns depend mainly on the horizontal distance between the foils, while the intensity of the mutual interaction between the wake vortices depends on the vertical distance. Thus, the propulsive characteristics of the dual fish-like foils are the complicated functions of the vertical and horizontal distances between the foils.

The present method has the limitation of potential-low assumption. However, if the foils are only undulating the rear parts of the body and flow separation near the leading edge of the foils does not occur, the present method can be applied to the design of biomimetic fish-like propulsors or vehicles.

Acknowledgement

This work was supported by Korea Research Foundation Grant funded by Korea Government (The Ministry of Education & Human Resources Development, Basic Research Promotion Fund) (KRF-2005-206-D00007). This work was also supported by Grant No. (R01-2005-000-10310-0) from the Basic Research Program of the Korean Science and Engineering Foundation.

References

[1] K. V. Rozhdestvensky and V. A. Ryzhov, Aerohydrodynamics of flapping-wing propulsors, *Progress in Aerospace Sciences* 39 (2003) 585-633.

[2] S. Ho, H. Nassef, N. Pornsinsirirak, Y-C. Tai, and C-M. Ho, Unsteady aerodynamics and flow control for flapping wing flyers, *Progress in Aerospace Sciences* 39 (2003) 635-681.

[3] M. Sfakiotakis, D. M. Lane, J.B.C. Davies, Review of fish swimming modes for aquatic locomotion, IEEE *Journal of Oceanic Engineering* 24 (2), (1999) 237-252.

[4] P. R. Bandyopadhyay, Trends in biorobotic autonomous undersea vehicles, *IEEE J. Oceanic Eng.* 30 (2005) 109-139.

[5] M. S. Triantafyllou, A. H. Techet and F.S. Hover, Review of experimental work in biomimetic foils, *IEEE Journal of Oceanic Engineering* 29 (3) (2004) 585-594.

[6] R. Knoller, Die gesetze des lufwiderstandes, *Flug- und Motortechnik(Wien)* 3 (21) (1909) 1-7.

[7] A. Betz, Ein beitrag zur erklarung des segelfluges, *Zeitschrift fur Flugtechnik und Motorluftschiffahrt* 3 (1912) 269-272.

[8] K. D. Jones, C. M. Dohring and M. F. Platzer, Wake structures behind plunging airfoils: a comparison of numerical and experimental results, *AIAA 1996-0078*.

[9] K. D. Jones and M. F. Platzer, An experimental and numerical investigation of flapping-wing propulsion, *AIAA 1999-0995*.

[10] J. C. S. Lai and M. F. Platzer, Jet characteristics of a plunging airfoil, *AIAA Journal*. 37 (12) (1999) 1529-1537.

[11] K. D. Jones, B. M. Castro, O. Mahmoud, and M. F. Platzer, A numerical and experimental investigation of flapping-wing propulsion in ground effect, *AIAA 2002-0866*.

[12] C. Han, H. J. Lee, J. Cho, Numerical study of biomimetic foil propulsion, *Transactions of the KSME Part B*. 30 (9) (2006) 866-872.

[13] D. Weihs, Hydromechanics of fish schooling. *Nature (London)*, 241 (1973) 290-291.

[14] D. Weihs, P. W. Webb, Optimization of locomotion. *Fish Biomechanics* (Edited by Webb P. W. and Weihs D.) Praeger New York (1983) 339-371.

[15] P. R. Bandyopadhyay, J. M. Castano, W. H. Nedderman, and M. J. Donnelly. Experimental simulation of fish-inspired unsteady vortex dynamics on a rigid cylinder, *ASME J. Fluids Eng.* 122 (2000) 219-238.

[16] M. Akiyama, K. Takato, T. Tsutsui, H. Sugiyama, and N. Ninimiya, Flow around vibrating elastic plates, Proceedings of the 6th Asian Symposium On Visualization, May 28-31 Pusan Korea, (2001) 79-81.

[17] C. Han, J. Cho, Unsteady aerodynamics analysis of flat plates in pitch oscillation, *AIAA Journal* 20 (6) (2006) 1121-1126.

[18] J. Katz and A. Plotkin, Low-Speed Aerodynamics, 2nd Edition, Cambridge University Press, 40 West 20th Street, New York NY 10011-4211 USA (2001) Chap. 13.

[19] D. T. Mook, S. Roy, G. Choksi and B. Dong, Numerical simulation of the unsteady wake behind an airfoil, *Journal of Aircraft* 26 (6) (1989) 509-514.

[20] I. H. Tuncer and K. Mustafa, Thrust generation caused by flapping airfoils in a biplane configuration, *Journal of Aircraft* 40 (3) (2003) 509-515.

[21] J. Yan, R. Wood, S. Avandhanula, R. Sitti, and R. S. Fearing, Towards flapping wing control for a micromechanical flying insect, IEEE International Conference on Robotics and Automation, The IEEE Robotics and Automation Society Seoul Korea (2001) 3901-3908.